Dynamics of wall bounded flow

Ozan Tuğluk and Hakan I. Tarman

Department of Engineering Sciences, Middle East Technical University, Ankara, Turkey {tugluk, tarman}@metu.edu.tr

There are various scenarios proposed in literature for transition in plane channel (Poiseuille) flow. In this work, one of these scenarios, namely, streak breakdown, is tested numerically using a Karhunen-Loeve (K-L) based model. The K-L basis was empirically generated earlier using a numerical database representing the flow. This basis is modified in this work to include the mean flow. A K-L basis provides an optimal parametrization of the underlying flow in energy norm. Since it is specific to the flow, each basis element carries an independent characteristic of the flow and has physical interpretation. A system of model amplitude equations is then obtained by Galerkin projection of the governing equations onto the space spanned by the K-L basis. The physical interpretation of the basis elements is used to truncate the resulting system to obtain a low dimensional model.

1 Introduction

Despite much research and progress, there is still a lack of complete picture of transition to turbulence in the wall-bounded flows. This is also true in the case of plane channel (Poiseuille) flow which is a very attractive flow to study the dynamics of transition due to its simple geometry. It started with the conflict between the linear stability analysis leading to famous Orr-Sommerfeld equation predicting stability for Reynolds number $Re < 5572$ [OP83] and experimental observations showing transition to turbulence for Re as low as 1000 [PH69]. This conflict motivated much research on nonlinear analysis and various transition scenarios [RSBH98].

A recent theory on transition through transient growth of disturbances before decaying is supported by experiments and numerical simulations and is to play a fundamental role in the initial stages of transition [Kli92, RH93]. In channel flows, the disturbances that yield the greatest transient growth, called optimals, are independent, or nearly independent, of the streamwise coordinate. Streamwise streaks periodic in the spanwise direction and their

Kenan Taş et al. (eds), Mathematical Methods in Engineering, 243–253.

subsequent breakdown leading to transition have been proposed as a transition scenario and investigated in [RSBH98].

In this preliminary study, the breakdown of streamwise streaks is numerically simulated using a low dimensional model reduced from the governing Navier-Stokes (NS) equations through Karhunen-Loéve (KL) procedure. This procedure is useful in studying complicated physical phenomena by decomposing an experimental or numerical realization of flow into structures (KL modes) each of which carries an independent character of the flow. This may be a static analysis in which the evolution of the flow is studied by projecting an existing database representing a spatial realization of the flow at discrete times onto the subspace spanned by the KL modes (KL subspace), [WHS97] or a dynamic analysis in which the evolution of the flow is studied by numerically integrating a relatively low dimensional model of the governing equations obtained by Galerkin projection onto the KL subspace [SZ92, Tar03]. Contrary to the static analysis being limited to the control parameter (such as Reynolds number) values at which the database is obtained, the dynamic analysis allows a study in a range of the parameter values.

2 Governing equations

In contrast to the boundary layer slowly growing in the streamwise directon over a flat plate, the channel flow between two parallel plates is homogeneous in both streamwise and spanwise directions after an entrance region in which both upper and lower boundary layers are growing. That is why channel flow has a special place in the experimental or numerical study of the transitional mechanisms. Channel flow is driven by a constant pressure gradient k in the x-direction in a geometry, $-\infty < x, z < \infty$; $-h < y < h$. Here, x is the streamwise direction, z the spanwise direction and y the direction between the parallel plates. For velocity and spatial coordinates, the symbols, $\mathbf{u} = (u_1, u_2, u_3) = (u, v, w)$ and $\mathbf{x} = (x_1, x_2, x_3) = (x, y, z)$ will be used interchangibly.

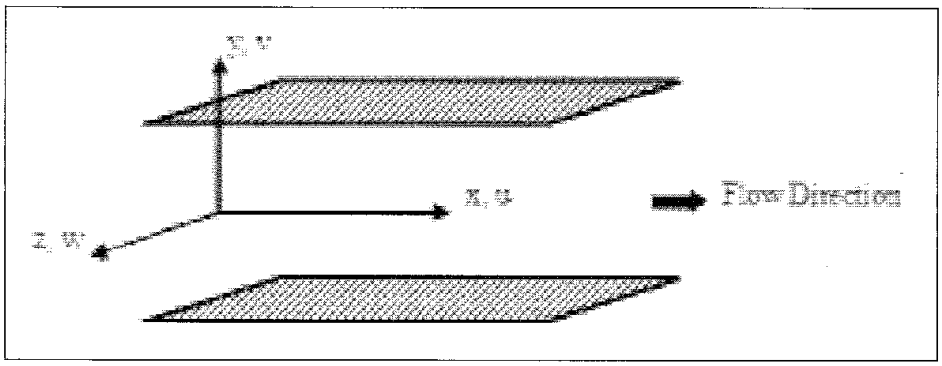

Fig. 1. Flow geometry and the notation

The governing Navier-Stokes (NS) equations and the boundary conditions are:

$$\frac{\partial u_j}{\partial x_j} = 0, \tag{1a}$$

$$\frac{\partial u_i}{\partial t} + \frac{\partial}{\partial x_j} u_i u_j + \frac{\partial p}{\partial x_i} = \delta_{i1} + \frac{1}{R_\tau} \nabla^2 u_i \tag{1b}$$

for $i = 1, 2, 3$, and

$$\mathbf{u}(x, -1, z, t) = \mathbf{u}(x, 1, z, t) = 0 \tag{2}$$

with periodic boundary conditions in the x and y directions. Here, the standard normalization is used, based on the friction velocity $u_\tau = \sqrt{kh/\rho}$ and $R_\tau = \frac{u_\tau h}{\nu}$ is the Reynolds number [TL72].

3 KL procedure

KL modes are computed as eigenfunctions, $\{\Phi^{(n)}\}$, of the integral equation :

$$\int_V K_{ij}(\mathbf{x}, \mathbf{x}')\, U_j^{(n)}(\mathbf{x}')\, d\mathbf{x}' = \lambda_n U_i^{(n)}(\mathbf{x}) \tag{3}$$

whose kernel is the two-point correlation tensor

$$K_{ij}(\mathbf{x}, \mathbf{x}') = \frac{1}{K} \sum_{k=1}^{K} u_i^{(k)}(\mathbf{x})\, u_j^{(k)}(\mathbf{x}') \tag{4}$$

obtained using flow database

$$\mathbf{u}_i^{(k)}(x, y, z) = \mathbf{u}_i(x, y, z, k\Delta t) \qquad k = 1, 2 \cdots K, \quad i = 1, 2, 3. \tag{5}$$

Since the flow is taken as periodic in the x and z directions, KL modes take the form

$$\mathbf{U}^{(\mathbf{m})}(\mathbf{x}) = e^{2\pi i \left(\frac{mx}{L_x} + \frac{nz}{L_z}\right)} \mathbf{V}^{(q)}(m, n; y) \tag{6}$$

where $\mathbf{m} = (m, n, q)$ is an index vector. KL modes form an orthogonal basis in an inner product space

$$\left(\mathbf{U}^{(n)}, \mathbf{U}^{(m)}\right)_{\mathbf{x}} \equiv \int_V \sum_{j=1}^{3} U_j^{(\mathbf{n})}(\mathbf{x}) U_j^{(\mathbf{m})}(\mathbf{x}) dV = \delta_{\mathbf{nm}}, \tag{7}$$

and represent the flow in an expansion

$$\mathbf{u}(\mathbf{x}, t) = \sum_{\mathbf{m}} a_{\mathbf{m}}(t)\, \mathbf{U}^{(\mathbf{m})}(\mathbf{x}), \tag{8}$$

where the expansion coefficients are statistically independent in time,

$$(a_{\mathbf{m}}, a_{\mathbf{n}})_t \equiv \frac{1}{K}\sum_{k=1}^{K} a_{\mathbf{m}}(k\Delta t)\; a_{\mathbf{n}}(k\Delta t) = \lambda_{\mathbf{m}}\delta_{\mathbf{nm}}. \tag{9}$$

Due to the symmetries in flow geometry [WHS97], KL modes come out degenerate as such

$$\lambda_{(m,n,q)} = \lambda_{(m,-n,q)} = \lambda_{(-m,n,q)} = \lambda_{(-m,-n,q)}. \tag{10}$$

Consequently, KL modes need to be computed only for the positive index pair (m, n), $m, n > 0$, the other members of the index family $\{m, n, q\}$, where

$$\{m,n,q\} \equiv \{\underbrace{(m,n,q),(-m,-n,q)}_{\text{conjugate pairs}};\underbrace{(m,-n,q),(-m,n,q)}_{\text{conjugate pairs}}\} \tag{11}$$

are obtained using the symmetry relations. KL modes satisfy all the spatial constraints, such as continuity equation, boundary conditions and form the building blocks of the flow

$$\mathbf{v}^{(\mathbf{m})}(\mathbf{x},t) \equiv \underbrace{a_{(m,n,q)}(t)\mathbf{U}^{(m,n,q)}(\mathbf{x}) + a_{(-m,-n,q)}(t)\mathbf{U}^{(-m,-n,q)}(\mathbf{x})}_{\text{complex conjugate pairs}} + \underbrace{a_{(-m,n,q)}(t)\mathbf{U}^{(-m,n,q)}(\mathbf{x}) + a_{(m,-n,q)}(t)\mathbf{U}^{(m,-n,q)}(\mathbf{x})}_{\text{complex conjugate pairs}} \tag{12}$$

for each index family $\{m, n, q\}$.

These computed KL modes, as they satisfy spatial constraints and carry independent features of the flow, form a convenient basis for reducing NS equations to a relatively low dimensional dynamical system via Galerkin projection. Further, their divergence-free nature causes the gradiant term to drop during projection. In order to construct a relatively low dimensional KL based dynamical model of the governing equations, first, an approximation of the flow

$$\mathbf{u} \approx \mathbf{u}_s = \sum_{\mathbf{n}\in S} \mathbf{v}^{(\mathbf{n})}(\mathbf{x},t) \tag{13}$$

in terms of a set of KL modes selected based on their physical importance is to be obtained. Here, S denotes index set of the selected KL modes. This approximation is, in turn, forced to satisfy the governing NS equations ($\mathrm{NS}(\mathbf{u}) = 0$) using Galerkin projection

$$\left(\mathbf{U}^{(\mathbf{m})}, \mathrm{NS}(\mathbf{u}_s)\right)_{\mathbf{x}} = 0 \tag{14}$$

resulting in a dynamical system

$$\frac{d}{dt}a_{\mathbf{m}} = PROD(\mathbf{m}) + \frac{1}{R_\tau}DISS(\mathbf{m};\mathbf{n})a_{\mathbf{n}} + NLIN(\mathbf{m};\mathbf{n},\mathbf{r})a_{\mathbf{n}}a_{\mathbf{r}}, \qquad (15)$$

where, using the index vector representations $\mathbf{m} = (m_1, m_3, q_m)$, $\mathbf{n} = (n_1, n_3, q_n)$ and $\mathbf{r} = (r_1, r_3, q_r)$, the coefficients are

$$PROD(\mathbf{m}) = \left(\mathbf{U}^{(\mathbf{m})}, \delta_{i1}\right)_{\mathbf{x}}, \qquad (16)$$

for $m_1 = m_3 = 0$,

$$DISS(\mathbf{m};\mathbf{n}) = \left(\mathbf{U}^{(\mathbf{m})}, \Delta\mathbf{u}_s\right)_{\mathbf{x}}, \qquad (17)$$

for $m_1 = n_1$, $m_3 = n_3$, and

$$NLIN(\mathbf{m};\mathbf{n},\mathbf{r}) = \left(\mathbf{U}^{(\mathbf{m})}, \mathbf{u}_s \times (\nabla \times \mathbf{u}_s)\right)_{\mathbf{x}} \qquad (18)$$

for $m_1 = n_1 + r_1$, $m_3 = n_3 + r_3$. In the computation of the coefficients, $NLIN(\mathbf{m};\mathbf{n},\mathbf{r})$, the use of the equivalent form

$$\mathbf{u}\cdot\nabla\mathbf{u} = \frac{1}{2}(\mathbf{u}\cdot\mathbf{u}) - \mathbf{u}\times(\nabla\times\mathbf{u}) \qquad (19)$$

of the nonlinear term of NS equations is observed to improve the computation as verified by the satisfaction of the triad relation

$$NLIN(\mathbf{m};\mathbf{n},\mathbf{r}) + NLIN(-\mathbf{n};-\mathbf{m},\mathbf{r}) + NLIN(-\mathbf{r};\mathbf{n},-\mathbf{m}) = 0 \qquad (20)$$

where $-\mathbf{m} = (-m_1, -m_3, q_m)$.

4 Numerical procedure

NS equations are numerically integrated in [WHS97] by using Fourier-Chebyshev spectral method in which the flow is taken periodic in x and z directions. The flow variables are expanded in the form

$$\mathbf{u}(\mathbf{x},t) = \sum_{m=-\frac{M}{2}}^{\frac{M}{2}-1}\sum_{n=-\frac{N}{2}}^{\frac{N}{2}-1}\sum_{p=0}^{P}\hat{\mathbf{u}}(m,n,p;t)\,T_p(x_2)e^{ik_1x_1}e^{ik_3x_3} \qquad (21)$$

where $k_1 = 2\pi m/L_x$, $k_3 = 2\pi n/L_3$ and $T_p(y)$ are the Chebyshev polynomials. The values $L_x = \pi$, $L_z = 0.3\pi$, $P = 128$, $M = 48$, $N = 24$, $R_\tau = 135.5$ are selected based on the work [JM90] which corresponds to the minimal channel geometry to obtain turbulent flow at both upper and lower boundary layers.

Table 1. KL modes as computed in [WHS97]

KL mode $\mathbf{m} = (m, n, q)$	(0,1,1)	(0,1,2)	(1,1,1)	(1,1,2)	(0,1,3)	(0,1,4)
Energy content % $\lambda_{\mathbf{m}} / \sum_{\mathbf{n}} \lambda_{\mathbf{n}}$	13	10	5	5	3	2

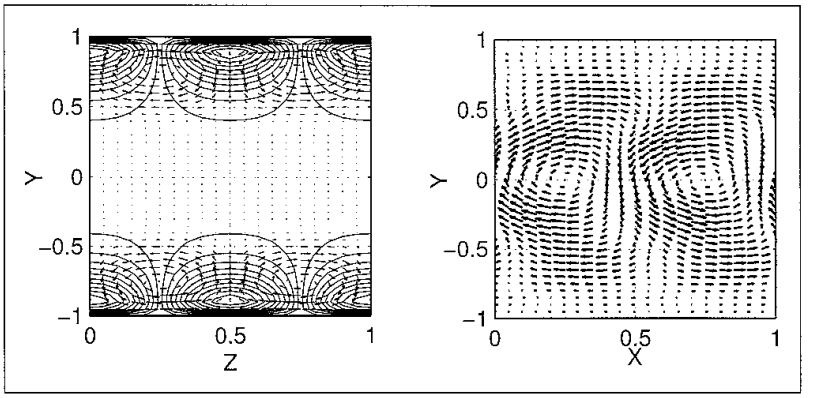

Fig. 2. Flow structure of KL modes (0,1,1) and (1,0,1)

The computed flow field after the removal of the mean flow is used to compute the KL modes as shown in Table 1. Each KL mode carries an independent feature of the flow.
For example, the most energetic KL mode $\mathbf{m} = (0, 1, 1)$, along which carries 13% of the flow energy, physically represents a pair of counter-rotating rolls extending in the streamwise direction in the upper and lower sections of the channel as shown in Figure 2. This rolling motion carries the fluid from the center towards the wall regions. KL modes are classified in [WHS97] as roll modes $(m = 0, n \neq 0, q)$, core or propagating modes $(m \neq 0, n, q)$, and net-flux modes $(m = 0, n = 0, q)$ depending on their physical roles. They vary with respect to the quantum number q in a way of increasing complexity in y-direction as shown in Figure 3. As q increases KL modes exhibit smaller scale structures and form symmetric and anti-symmetric pairs in the plane $y = 0$. This form necessitates the inclusion of KL modes in pairs in the set S.

In this work, the KL modes are re-computed in a way to include the mean flow which was removed in [WHS97]. This eliminates the need to model the mean flow, which would result in a cubic nonlinear term in the dynamical system. The inclusion of the mean flow in the extraction process of the KL modes effects only the net-flux modes $\mathbf{m} = (0, 0, q)$, especially the most energetic mode $\mathbf{m} = (0, 0, 1)$. As shown in Figure 3, $\mathbf{m} = (0, 0, 1)$ mode is in a form very similar to the mean profile.

The resulting dynamical system is numerically integrated in time for various forcing parameter R_τ values and for a selected set S of KL modes. Numerical solution is in turn used for a nonlinear stability analysis in two stages. In the first stage, the stability of the laminar flow, $U(y) = \frac{1}{2} R_\tau (1 - y^2)$, is numerically tested againts disturbances having no streamwise variation $(m = 0)$ at

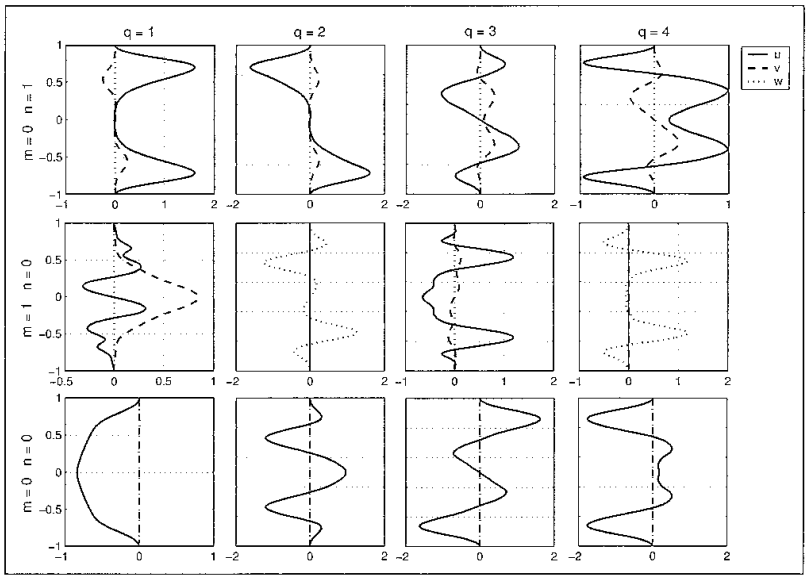

Fig. 3. Vertical profiles of KL modes $\mathbf{V}^q(m, n; y)$ (real part)

various R_τ values and the secondary flow , to which the laminar flow looses its stability, is obtained. In the second stage, the stability of the secondary flow is tested against disturbances that have streamwise variation ($m \neq 0$) through a numerical perturbation procedure. In this study, the (kinetic) energy of the flow

$$E(\mathbf{u}) = \frac{1}{2} \int_0^{L_z} dz \int_0^{L_x} dx \int_{-1}^{1} dy\, \mathbf{u} \cdot \mathbf{u} \tag{22}$$

relative to that of laminar flow ($E(U(y)\delta_{i1}) = 2L_xL_zR_\tau/15$), relative energy,

$$\varepsilon(\mathbf{u}) = \frac{E(\mathbf{u})}{2L_xL_zR_\tau/15} \tag{23}$$

is used as a measure.

In this work, KL modes that are thought to play the most important role in the transition process, are selected as:

$$S = \{(m, n, q) \mid (0, 0, 1 \cdots 25); (0, 1, 1 \cdots 4); (1, 0, 1 \cdots 4); (1, 1, 1 \cdots 4)\}.$$

Here, the main idea in the the inclusion of the $(0, 0, q)$ modes with $1 \leq q \leq 25$ is to have as complete representation of the modes carrying the flow energy as possible in the dynamical model system. Moreover, the parabolic laminar flow profile $U(y)$ is included in the system through the projection onto these modes

$$a_{\mathbf{m}}(t) = (\mathbf{U}^{\mathbf{m}}\,,\, U(y)\delta_{i1})_{\mathbf{x}} \quad \text{for} \quad \mathbf{m} = (0, 0, q) \in S. \tag{24}$$

Other modes are included in pairs $(q = 1; 2), (q = 3; 4)$ due to the appearance of the modes in pairwise symmetric and antisymmetric form around $y = 0$ plane (see Figure 3). Furthermore, the number of modes, $1 \leq q \leq 4$, is included

to provide the necessary degrees of freedom for the highly resolved KL modes to adjust to the low resolution requirements at low R_τ values. Recall that KL modes carry high vertical resolution due to their construction from data at high R_τ values ($R_\tau = 135.5$ in this case).

The dynamical model system is also an initial value problem. In the first stage of the two stage nonlinear stability analysis, an initial value of

$$a_{(m,n,q)}(t=0) = \begin{cases} A_0 & \text{for} \quad (m=0, n \neq 0, q) \in S \\ 0 & \text{otherwise} \end{cases} \tag{25}$$

is taken for the streamwise independent components $(m = 0, n \neq 0, q) \in S$ of the flow which is superimposed onto the laminar flow $(m = 0, n = 0, q) \in S$ of Eq. 24. Here, A_0 is selected for the relative energy $\varepsilon\left(\mathbf{u}(t=0)\right) = \varepsilon_0^0$ to take a particular value ε_0^0 . In the second stage, the initial value of

$$a_{(m,n,q)}(t=0) = \begin{cases} A_0 & \text{for} \quad (m=0, n \neq 0, q) \in S \\ A_1 & \text{for} \quad (m \neq 0, n, q) \in S \\ 0 & \text{otherwise} \end{cases} \tag{26}$$

is taken for the secondary flow arising from the first stage, $(m = 0, n, q) \in S$, and for the superimposed streamwise dependent component of the flow, $(m \neq 0, n, q) \in S$. Here, A_0 and A_1 are selected for the relative energy, $\varepsilon\left(\{\mathbf{u}(t=0) \mid A_1 = 0\}\right) = \varepsilon_0^0$ and $\varepsilon(\mathbf{u}(t=0) \mid A_0 = 0) = \varepsilon_1^0$ take separate particular values, ε_0^0 and ε_0^1 .

5 Results

In Figure 4, a typical solution obtained at $R_\tau = 20$ is shown. This solution, obtained at the particular initial relative energy value of $\varepsilon_0^0 = 10^{-2}$, shows that the laminar flow modeled by the system is stable at $R_\tau = 20$. The solution obtained at various other particular values of ε_0^0 supports the same conclusion. In another numerical experiment (Figure 5) at $R_\tau = 40$ and $\varepsilon_0^0 = 10^{-2}$, the laminar flow loses its stability to give rise to a secondary flow. The response of the system to the perturbation is shown as a burst in energy initially. Later, the flow reaches an equilibrium as a result of the dissipative effects of the nonlinear terms activated by the initial burst.

The secondary flow is characterized by the transfer of high momentum at the centre towards the wall layers. This can be seen in Figure 6(a) in the relative flattness of the mean secondary flow profile due to this momentum transfer in comparison to the laminar flow profile. A detailed look at the secondary flow profile in Figure 6(b) shows the streamwise high and low velocity streaks extending in the streamwise direction in the wall region. This is in accordance with the streamwise streak formation in literature.

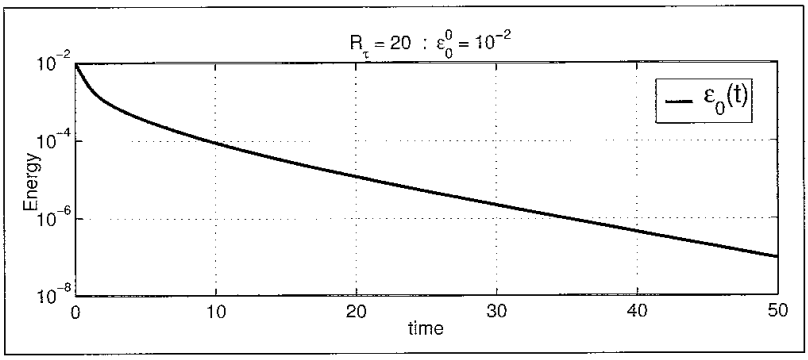

Fig. 4. The solution obtained at the particular R_τ and ε_0^0 values indicated.

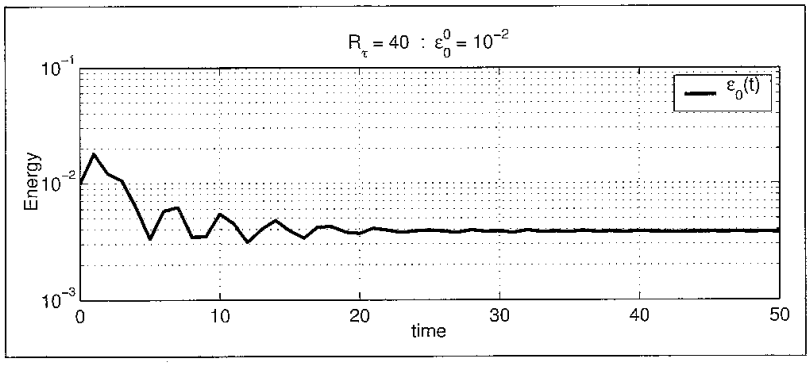

Fig. 5. The solution obtained at the particular R_τ and ε_0^0 values indicated.

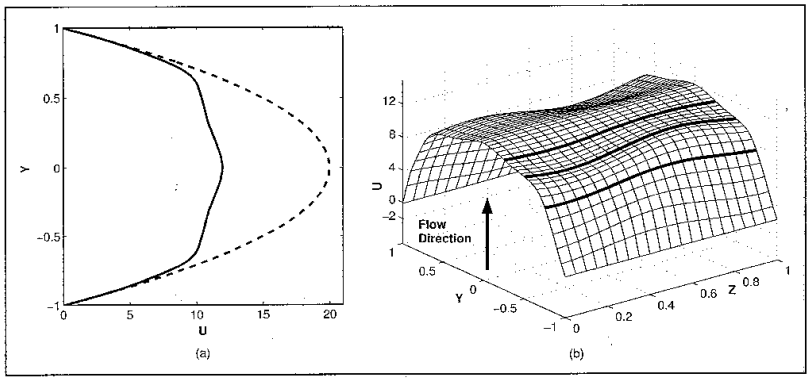

Fig. 6. (a) The comparison between the laminar flow and the mean secondary flow profiles obtained by the perturbation of the laminar flow at $R_\tau = 40$. (b) The highlighted curves indicate the spanwise variation in the streamwise velocity component of the flow. At each point on these curves, the value of the streamwise velocity component extend in the streamwise direction wihout varying, thus forming the streamwise high and low velocity streaks.

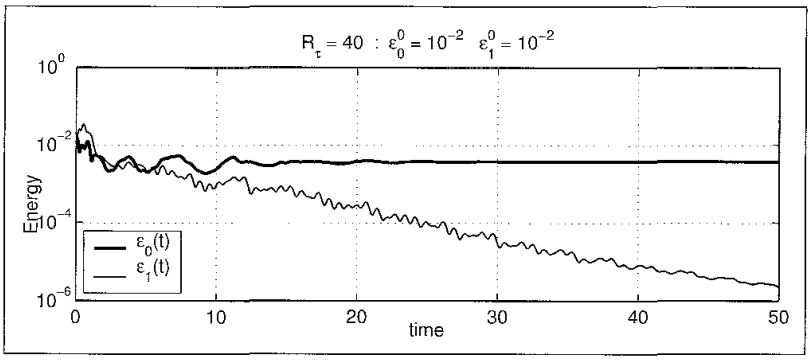

Fig. 7. The solution obtained at the particular R_τ and ε_0^0, ε_1^0 values indicated.

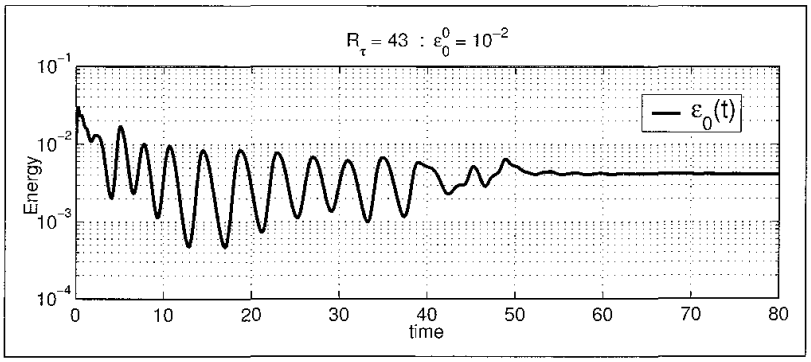

Fig. 8. The solution obtained at the particular R_τ and ε_0^0 values indicated.

The perturbation of the secondary flow obtained at $R_\tau = 40$ by three dimensional components of the flow shows the stability of the secondary flow (Figure 7). The numerical experiments at various other ε_1^0 values supports the same conclusion. Laminar flow, when perturbed at $R_\tau = 43$ and at various relative energy values ε_0^0 similarly loses its stability and gives rise to secondary flow. A typical solution for $\varepsilon_0^0 = 10^{-2}$ is shown in Figure 8. The secondary flow at $R_\tau = 43$ loses its stability to perturbations by three dimensional components of the flow (Figure 9). The numerical experiments at various other ε_1^0 values supports the same conclusion. This result is in agreement with the scenario of transition in literature through the breakdown of high and low velocity streamwise streaks.

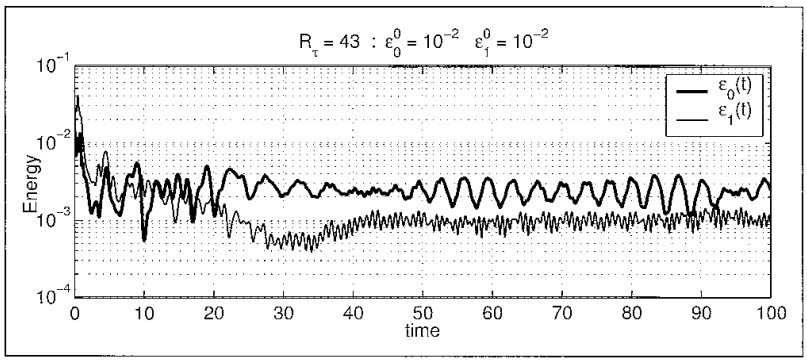

Fig. 9. The solution obtained at the particular R_τ and ε_0^0, ε_1^0 values indicated.

References

[OP83] Orszag, S.A., Patera, A.T.: Secondary instability of wall-bounded shear flows. Journal of Fluid Mechanics, **128**, 347-360 (1983)

[PH69] Patel, V.C., Head, R.: Some observations on skin friction and velocity profiles in fully developed pipe and channel flows. Journal of Fluid Mechanics, **38**, 181-201 (1969)

[RSBH98] Reddy, S.C., Schmid, P.J., Bagget, J.S., Henningson, D.S.: On stability of streamwise streaks and transition tresholds in plane channel flows, Journal of Fluid Mechanics, **365**, 269-303 (1998)

[Kli92] Klingmann, B.G.B.: On transition due to three-dimensional disturbances in plane Poiseuille flow. Journal of Fluid Mechanics, **240**, 167-195 (1992)

[RH93] Reddy, S.C., Henningson, D.S.: Energy growth in viscous channel flows. Journal of Fluid Mechanics, **252**, 209-238 (1993)

[WHS97] Webber, G.A., Handler, R.A., Sirovich, L.: Karhunen Loéve decomposition of minimal channel flow. Physics of Fluids, **9**, 1054-1066 (1997)

[SZ92] Sirovich, L., Zhou, X.: Coherence and chaos in a model of turbulent boundary layer. Physics of Fluids, **4**, 2855-2870 (1992)

[Tar03] Tarman, I.H.: A Karhunen-Loéve-based approach to numerical simulation of transition in Rayleigh-Benard convection. Num. Heat Transfer B., **43**, 567-586 (2003)

[TL72] Tennekes, H., Lumley, J.L.: A First Course in Turbulence. The MIT Press, Massachusetts (1972)

[JM90] Jiménez, J., Moin, P.: The minimal flow unit in near-wall turbulence. Journal of Fluid Mechanics, **225**, 213-240 (1990)